

Original Article

Atomic Force Microscopy (AFM) Analysis of an Object Larger and Sharper than the AFM Tip

Zhe Chen^{1,2}, Jiawei Luo^{1,2}, Ivo Doudevski², Sema Erten² and Seong H. Kim^{1,2*}

¹Department of Chemical Engineering, Pennsylvania State University, University Park, PA 16802, USA and ²Materials Research Institute, Pennsylvania State University, University, University Park, PA 16802, USA

Abstract

Atomic force microscopy (AFM) is typically used for analysis of relatively flat surfaces with topographic features smaller than the height of the AFM tip. On flat surfaces, it is relatively easy to find the object of interest and deconvolute imaging artifacts resulting from the finite size of the AFM tip. In contrast, AFM imaging of three-dimensional objects much larger than the AFM tip height is rarely attempted although it could provide topographic information that is not readily available from two-dimensional imaging, such as scanning electron microscopy. In this paper, we report AFM measurements of a vertically-mounted razor blade, which is taller and sharper than the AFM tip. In this case, the AFM height data, except for the data collected around the cutting edge of the blade, reflect the shape of the AFM tip. The height data around the apex area are effectively the convolution of the AFM tip and the blade cutting edge. Based on computer simulations mimicking an AFM tip scanning across a round sample, a simple algorithm is proposed to deconvolute the AFM height data of an object taller and sharper than the AFM tip and estimate its effective curvature.

Key words: atomic force microscopy, deconvolution, razor blade, sharpness, topography

(Received 11 February 2019; revised 6 May 2019; accepted 18 June 2019)

Introduction

Since its invention in 1986 (Binnig et al., 1986), atomic force microscopy (AFM) has been widely used for topographical analysis of micro- and nano-scale features in a wide range of hard and soft materials. Compared with electron microscopy (EM), AFM can provide high-resolution three-dimensional (3D) topographic information, and the sample preparation requirements for AFM are minimal. However, AFM has certain disadvantages such as limited scan size and appearance of image artifacts (Ricci & Braga, 2004; Gołek et al., 2014).

The most common image artifact is the tip convolution effect, which is unavoidable because of the finite size of the AFM tip. If the sample is atomically flat, such as graphene basal plane (Lui et al., 2009), only the very end of the AFM tip makes contact with the sample. However, if the sample contains tall and steep features, the measured image can be very different from the true topography; this is because not only the tip end, but tip sides can also be in contact with the tall and sharp features on the sample surface (Ricci & Braga, 2004; Gołek, et al., 2014). Thus, the AFM image is often the convolution of the tip shape and the sample topography. This can be used as a calibration method to determine the AFM tip shape if a sample with well-defined topography is used (Montelius & Tegenfeldt, 1993; Atamny & Baiker, 1995; Hübner et al., 2003).

*Author for correspondence: Seong H. Kim, E-mail: shkim@engr.psu.edu
Cite this article: Chen Z, Luo J, Doudevski I, Erten S, Kim SH (2019) Atomic Force
Microscopy (AFM) Analysis of an Object Larger and Sharper than the AFM Tip. Microsc
Microanal. doi:10.1017/S1431927619014697

In order to obtain the true topography of the sample, several reconstruction algorithms have been reported (Reiss et al., 1990; Keller, 1991; Villarrubia, 1994, 1997) and some of them have been embedded into image processing software (Kondratov et al., 2017). These algorithms need the tip shape information independently obtained from EM, or they will rely on reserve imaging (Montelius & Tegenfeldt, 1993; Atamny & Baiker, 1995; Hübner, et al., 2003) or blind reconstruction (Dongmo et al., 2000; Tranchida et al., 2006; Flater et al., 2014). However, for the so-called "blind area", where tip-sample contact is absent, and the area where more than one contact point is involved, these reconstruction algorithms cannot be applied (Keller, 1991). An alternative and simpler approach would be to approximate the AFM tip apex with a simple geometric shape. Then the dimension of the sample topography can be obtained using geometrical relationship of the tip and the topographic feature of the sample (Allen et al., 1992; Severin et al., 2011; Winzer et al., 2012; Josep et al., 2014; Shen et al., 2017). Although this approach is relatively simple, it often requires a reference point (such as flat surface) for mathematical calculations, and the geometric shape assumption of the tip may cause a large error.

In this work, AFM is used to analyze a razor blade edge, which is taller and sharper than the AFM tip. The AFM images were compared with the scanning electron microscopy (SEM) images of the blade and the AFM tip. While the AFM images mainly reflect the shape of the AFM tip because the imaged object is larger and sharper than the AFM tip, the data obtained from the apex area of the blade edge represent the convolution of the blade edge radius and the apex shape of the AFM tip. Based on

© Microscopy Society of America 2019

2 Zhe Chen *et al.*

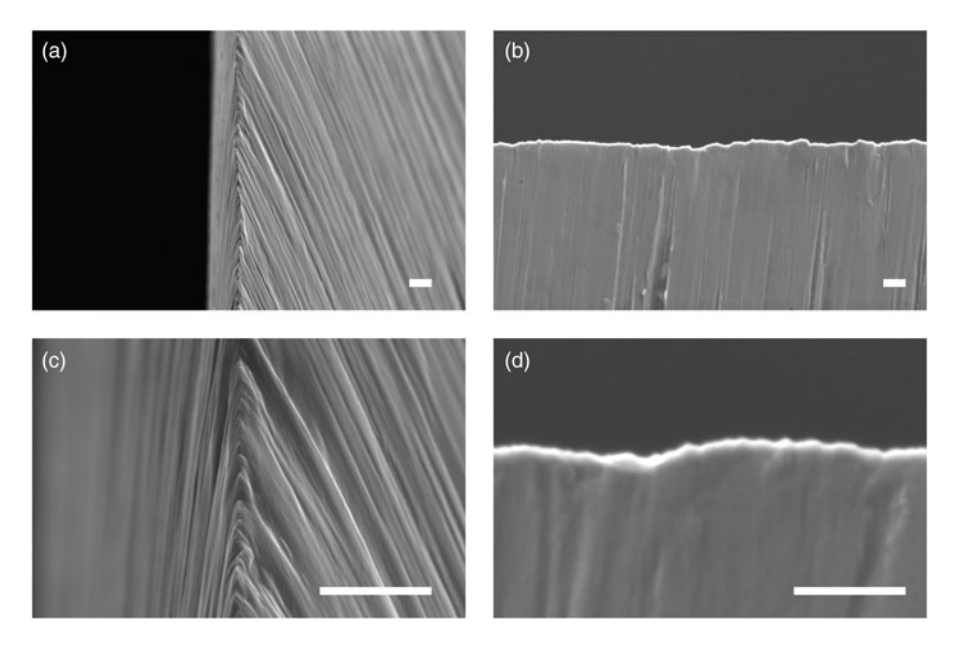


Fig. 1. SEM images of the blade when the blade is (a) vertically mounted with a 4° tilt angle and (b) horizontally mounted. c,d: Close-up images of (a) and (b), respectively. All the scale bars are 5 µm.

simulations of an AFM image for artificially well-defined tip scanning across a spherical shape sample, we propose a simple algorithm to estimate the effective curvature of the sharp razor blade edge. This algorithm can be applied to other tall and sharp samples.

Methods

Experimental

The samples used in this work are off-the-shelf commercial razor blades. AFM images were obtained using a Nanoscope V Dimension Icon AFM system (Bruker, Santa Barbara, CA) in the Peak Force Tapping (PFT) mode. AFM probes consisting of a Si tip on a Si₃N₄ cantilever with a nominal spring constant of 0.4 N/m (ScanAsyst-Air, Bruker, Santa Barbara, CA) were used for AFM imaging. The PFT mode was chosen for imaging because it can prevent the tip from blunting during the imaging scan. A PFT set point of 2 nN with a feedback gain of 35 was used for topographic scanning. The typical scan size was 6 μ m \times 6 μ m, and the scan speed was 12 μ m/s.

The SEM images of the razor blade and the AFM probe were taken using a Scios 2 SEM system (Thermo Fisher Scientific, Waltham, MA) with an electron beam voltage of 5–10 kV and a current of 0.2–0.4 nA, and a working distance of 15–18 mm.

Simulation of PFT Operation with Known Geometries

In order to show the tip shape convolution in the AFM imaging and test the algorithm for extraction of the effective curvature of the sample, the PFT imaging operation was simulated using Matlab $^{\circ}$. The tip and sample shapes were separately constructed in a matrix array of $1,000 \times 1,000$ pixels. Then, the tip matrix array moved toward the sample matrix along the vertical axis at a given horizontal pixel until two matrices touched each other at one point. The height of that position was registered. Then, the tip matrix was fully retracted and shifted horizontally by

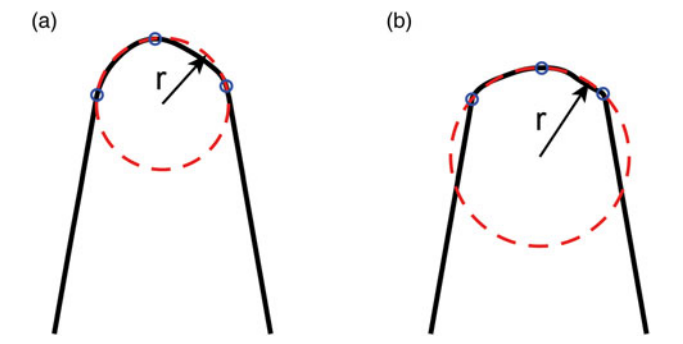
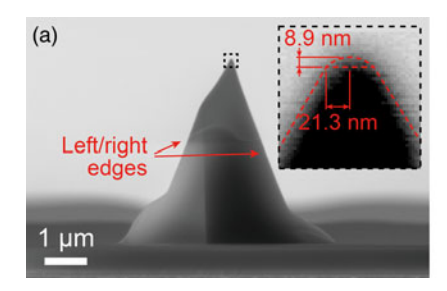


Fig. 2. Schematic illustration of (**a**) sharp and (**b**) blunt apex of razor blades. The radius of the red dashed circle, which can be defined as the effective curvature of the blade end, can be calculated mathematically from three data points (blue dots) marked along the apex.

one pixel. This process was repeated until the entire sample surface was imaged. The relative height information at each horizontal pixel location makes up the topography of the sample imaged with the tip.

Results and Discussion

Figure 1 shows SEM images of a razor blade when it is mounted along the electron beam axis with a 4° tilt angle (Figs. 1a, 1c) and perpendicular to the electron beam axis (Figs. 1b, 1d). The SEM images show that both sides of the blade have ground marks, and the blade edge is very sharp. The grinding process leaves nanoscale non-uniformity in the roughness of the blade sides, which results in local variations of the shape of the blade edge. In order to quantitatively assess the blade edge, its effective curvature can be defined as the radius of the circle going through the highest point in the middle and the points where two side walls start (Fig. 2). If one uses focused ion beam (FIB) to generate a cross-section, then the true curvature of the blade edge at that specific location could be measured using SEM. In order to obtain the



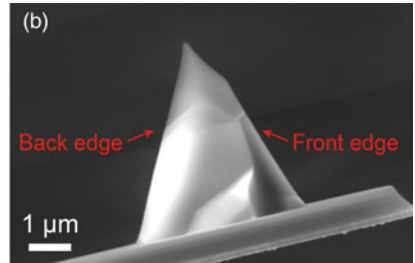


Fig. 3. SEM images of the AFM tip: (a) front view; the inset shows the details of the apex of the tip and (b) side view.

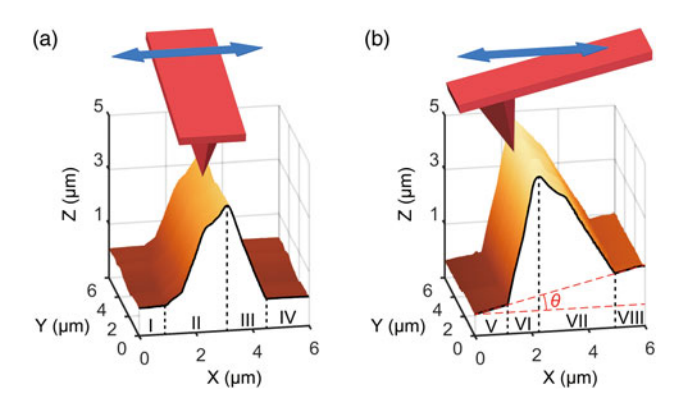


Fig. 4. 3D plot of AFM topographic image of the blade collected when the scan angle is (**a**) 90° where the AFM probe is parallel to the blade edge, and (**b**) 0° where the AFM probe is perpendicular to the blade edge. The line scan data in (**a**) and (**b**) show the cross-sections at the front of the blade image ($Y = 0 \mu m$).

average radius and its variation along the blade, the FIB-SEM imaging must be repeated stepwise along the blade. This process is extremely time-consuming and thus would be costly and inefficient. By using AFM to evaluate the topography of the blade edge and deconvolute the shape of the AFM tip, such issues can be avoided.

The SEM images of the front and side views of the AFM tip used for data collection are displayed in Figure 3. The height of the tip is about 4.4 μ m. The tip is in an asymmetric square pyramid shape. The side walls are not perpendicular to the plane of the cantilever. The tip apex could be fitted with a circular segment (Fig. 3a). Often, the radius of the tip is not as small as (or the same as) the nominal value provided by the manufacturer.

In topographic imaging with AFM, two scan directions were tested for the data collection and the collected 3D height images are shown in Figure 4 along with schematic illustration of the scan directions. The fast-scan direction of imaging is perpendicular to the blade edge (from left to right and vice versa). In Figure 4a, the long-axis of the AFM cantilever is parallel to the blade edge; therefore, the fast-scan direction is perpendicular to the cantilever axis (called the 90° scan direction). In Figure 4b, the long-axis of the AFM cantilever is perpendicular to the blade edge; therefore, the fast-scan direction is parallel to the cantilever axis (called the 0° scan direction). For further discussion, the cross-sectional line profiles at the front of the imaged blade are shown in Figures 4a and 4b.

For the 90° scan direction, the cross-sections of each scan along the fast-scan axis can be divided into four regions, which are marked as I, II, III, and IV in Figure 4a. The height is constant in region I, then it increases and reaches the highest

point in region II, then it decreases to the initial value in region III, and finally it remains constant again in region IV. By comparing the AFM images with the SEM images of the blade (Fig. 1c) and the AFM tip (Fig. 3a), it can be seen that the AFM cross-section follows the shape of the AFM tip, rather than the blade. It is noted that the tip height in the AFM image (Fig. 4a) is shorter than that in the SEM image (Fig. 3a). Considering that the AFM probe is tilted with the tip side pointing down because of the angle of the probe holder (which varies depending on the AFM instrument design), it can be envisioned that the end of the cantilever touches the blade when the tip is not in contact with the blade.

For the 0° scan direction, the cross-section profile can also be divided into four regions. To avoid ambiguity, these four regions are marked with V, VI, VII, and VIII in Figure 4b. In this case, the height increases linearly in region V, increases at a much faster rate in region VI, then decreases in region VII, and finally increases linearly at the starting rate again in region VIII. By comparing with the cross-section of the side view of the SEM image of the AFM tip (Fig. 3b), it is clear that the height profiles in regions VI and VII are identical with the back and front edges of the AFM tip, respectively. The straight line connecting regions V and VIII is the cantilever touching the blade. The tilt (θ) measured from the AFM cross-section is 13.5°, which is consistent with the angle of the probe holder of the AFM system used in this study, thus confirming that the cross-section is the reverse image of the AFM tip and cantilever.

Although most of the topographic information in AFM image reflects the shape (especially, side walls) of the AFM tip touched by the blade edge; the apex region of the topographic image where the AFM tip apex is touching the blade edge still carries the information of the blade end. However, as presented in Figure 3, the apex of the AFM tip cannot be considered as a sharp point, so the height data collected at the cutting edge of the blade are the convolution of the blade shape and the AFM tip apex. In order to investigate such convolution effects in AFM imaging, computer simulations mimicking the PFT scanning of an AFM tip across a well-defined shape were performed. Figure 5 illustrates two tip shapes—sharp versus blunt—used in the simulation; the scanned sample is a tall post with a round end (curvature = 150 nm).

For the simulation with an ideally sharp tip (Fig. 5a), the height profile of the sample consists of two tilted lines and an arc (Fig. 5c). In the height profile, the joint points of the tilted lines and the zero line are marked as A and E, the joint points of the arc and the tilted lines are marked as B and D, and the highest point at the middle point of the height profile is marked as C. The two tilted lines (AB and DE) reflect the side edges of the tip, and the arc (BCD) follows the true curvature of the sample (Fig. 5b).

4 Zhe Chen *et al.*

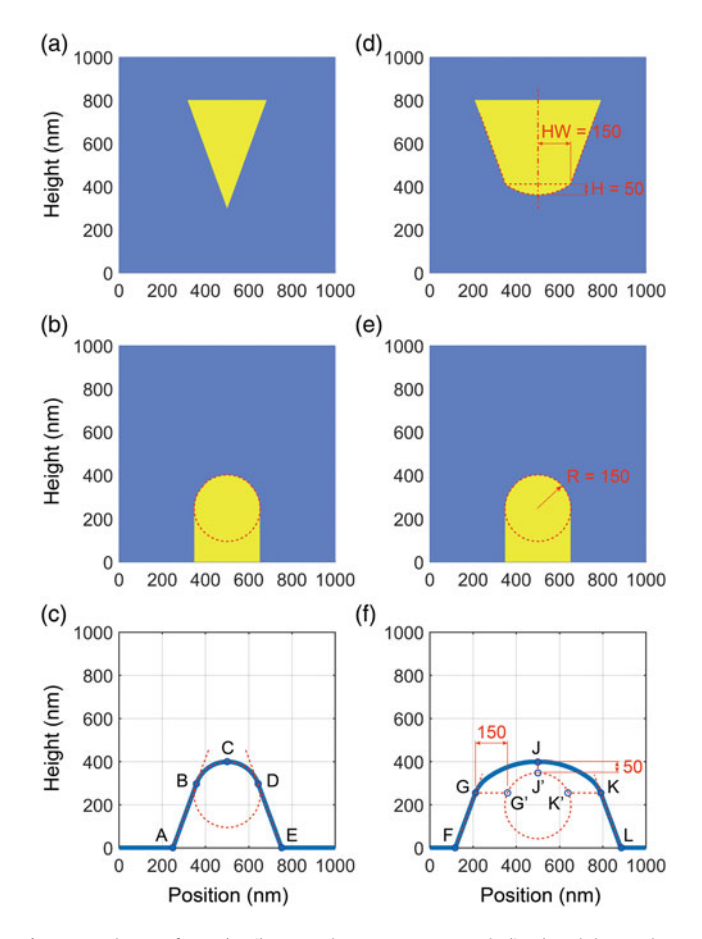


Fig. 5. Simulation of a tip (\mathbf{a}, \mathbf{d}) scanned across over a sample (\mathbf{b}, \mathbf{e}) and the resulting height profile (\mathbf{c}, \mathbf{f}) . \mathbf{a} : A sharp tip. \mathbf{d} : A blunt tip. The blunt tip consists of a trapezium and a circular segment. \mathbf{b} , \mathbf{e} : The same tall and round sample. \mathbf{c} , \mathbf{f} : The height profiles obtained with the sharp tip (\mathbf{a}) and the blunt tip (\mathbf{d}) , respectively.

In the simulation with a blunt tip (Fig. 5d), the tip shape convolution becomes significant. The shape of the blunt tip, which is presented in Figure 5d, is constructed based on the SEM image of the actual AFM tip (Fig. 3a). The sides of the isosceles trapezoid (tip side walls) are not parallel to the tangential line of the arc of the circular segment (tip end) at their meeting points. The height profile obtained with the blunt tip (Fig. 5f) can also be divided into two tilted lines (marked as FG and KL) and one curve (marked as GJK). Again, the two tilted lines (FG and KL) reflect the edges of the tip, which is similar to the case of the sharp tip; but the curve (GJK) is the convolution of the tip and sample curvatures.

By comparing the simulated height profile in Figure 5f with the topography of the imaged surface in Figure 5e, it can be seen that, at point G, the right side point of the circular segment of the tip is in contact with the sample (G'); at point J the lowest point of the tip is in contact with the sample (J'); and at point K the left side point of the tip circular segment is in contact with the sample (K'). Therefore, by moving point G to the right by a distance of the half width of the circular segment on the tip (HW in Fig. 5d), the point G', a point reflecting the topography of the sample, can be located. Similarly, by moving point J downward by the distance of the height of the circular segment (H in Fig. 5d) and moving point K to the left by the distance of the half width of the circular segment, point J' and point K' can be located, respectively. Points G', J', and K' are the true contact

points. Once three points of the true sample topography are found, a circle going through those three points can be defined and its radius can be calculated mathematically.

This algorithm can be used to determine three points on the true topography of the blade edge in the experimental AFM image, which allows estimating the effective curvature of the cutting edge of the blade as defined in Figure 2. Note that, unless the sample cross-section is perfectly circular, the arc going through the three points is not the actual topography of the blade edge (Fig. 2); nevertheless, it is still a good estimate of the local curvature (or sharpness) of the blade edge. Figure 6 shows the process to apply the algorithm described here and to obtain the local radius of a blade edge.

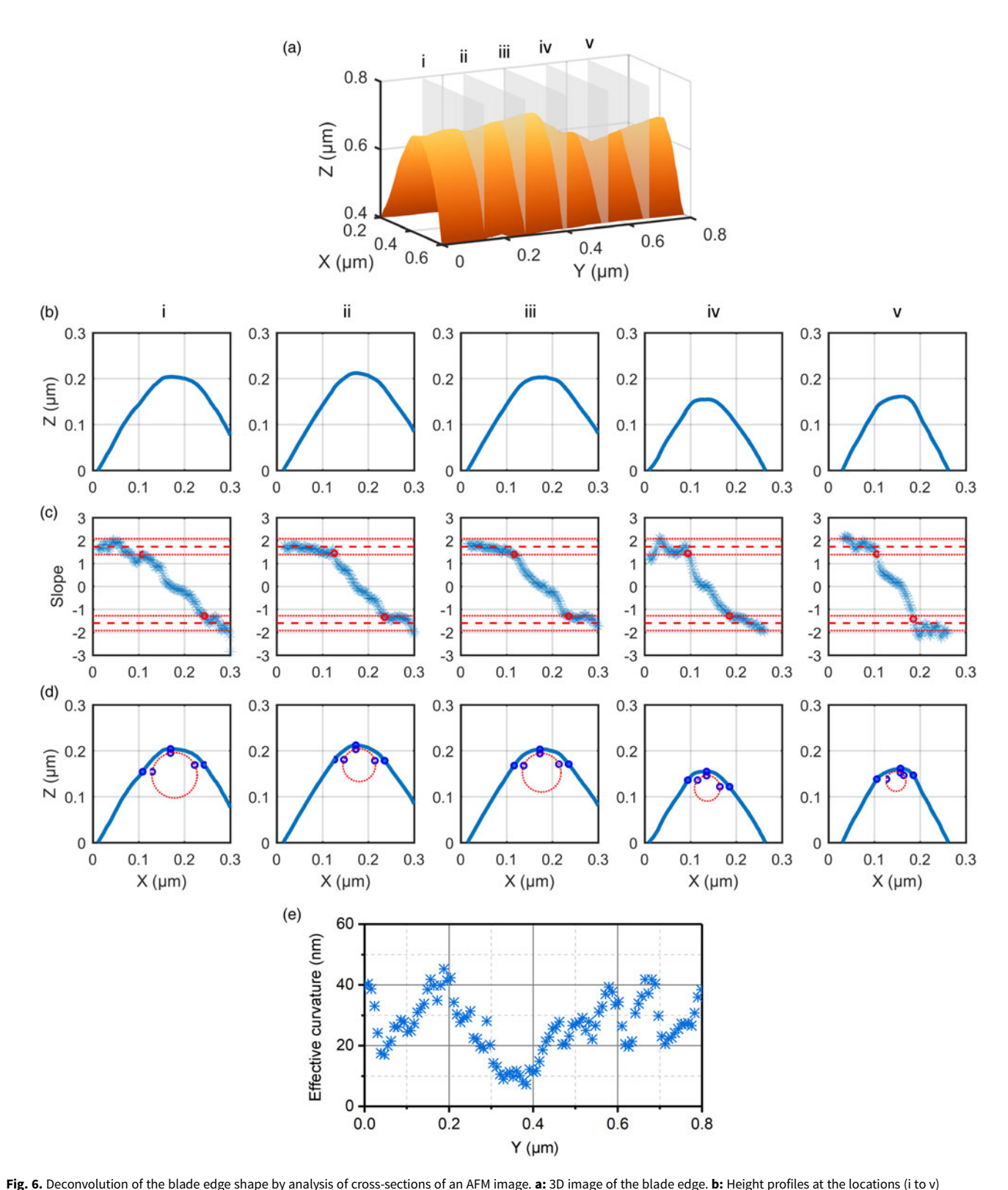
Figure 6a displays a 3D plot of the blade edge, and the crosssection height profiles of five locations marked as i through v are plotted in Figure 6b. The first step is to locate three points equivalent to GJK in Figure 5f. Locating the highest point (corresponding to J in Fig. 5f) is straightforward, but the joint points for the blade edge (corresponding to G and K in Fig. 5f) are not as obvious as in the case of simulation (Fig. 5). In order to determine the joint points, the tangential line of each point on the height profile is obtained and the slope of these tangential lines is plotted in Figure 6c. It is found that, for all the locations on the blade edge, the slope fluctuates around a positive constant value at first (the end of region II in Fig. 4a), decreases near the tip end region, and then fluctuates again around a negative constant value (the beginning of region III in Fig. 4a). The points where the slope begins and stops to change are the joint points G and K, respectively. Then, as shown in Figure 6d, by shifting the three points in the way shown in Figure 5f, three points of the blade cutting edge (corresponding to G', J', and K' in Fig. 5f) can be determined. A circle going through these three points can be obtained and the radius of the circle corresponds to the effective curvature (sharpness) of the blade cutting edge at that specific location. All data processing can be carried out numerically and automatically with simple programing. Figure 6e plots the variation in effective curvature of the cutting edge as a function of position along the blade. The average value of the effective curvature of the blade edge shown in Figure 6a is 27 ± 9 nm. This result is quite comparable with the previous results from FIB-SEM images (Scienceofsharp, 2015).

This work provides guidance for the topographical analysis of sharp and tall samples with AFM and puts forward a convenient method to estimate the sharpness of wide array of samples. The effective curvature of blade edge is a critical parameter for cutting tools, certain medical tools, and industrial razor blades. This method can be applied to any tall and sharp samples, and therefore it has a potential in practical applications, such as quality control, process control, and set-up tools, for nanoscale or microscale features and products.

Conclusion

This work demonstrated how AFM could be used to analyze the topography of a blade edge and determine the effective curvature of the blade edge. The AFM image is the convolution of the AFM tip and the blade edge. The AFM images mainly reflect the shape of the AFM tip due to the blade being taller and sharper than the AFM tip, except for the data collected around the apex of the blade edge. Based on the simulation of an AFM tip scanning across an ideal round sample, an algorithm is proposed to deconvolute the AFM images and extract the topography of the real

Microscopy and Microanalysis 5



marked in (a). c: Slope of each point on the cross-sections. The dashed lines represent the slope of the AFM tip side edges. Taking the tip mounting error into consideration, an error tolerance can introduced; in (c), the dotted lines represent a ±10% deviation of the AFM tip edge slope. d: Height profiles with the circle going through the three true contact points. e: The effective curvature of the blade edge as a function of position along the Y direction.

sample. In this algorithm, three true contact points are located after deconvolution of the AFM tip shape and dimension from the collected height data, which then are used to draw an arc in

order to describe the topography of the sample. This method can be applied to any 3D topographic features that are taller and sharper than AFM probes.

6 Zhe Chen *et al.*

Acknowledgments. This work was supported by the National Science Foundation (Grant No. CMMI-1727571).

Author contributions. S.H.K. and S.E. conceived the concept. Z.C., J.L., and I.D. designed and conducted AFM and SEM measurements. Z.C., I.D., and S.H.K. analyzed the data and wrote the manuscript.

References

- Allen MJ, Hud NV, Balooch M, Tench RJ, Siekhaus WJ & Balhorn R (1992).
 Tip-radius-induced artifacts in AFM images of protamine-complexed DNA fibers. Ultramicroscopy 42-44, 1095–1100.
- Atamny F & Baiker A (1995). Direct imaging of the tip shape by AFM. Surf Sci 323(3), L314–L318.
- Binnig G, Quate CF & Gerber C (1986). Atomic force microscope. *Phys Rev Lett* **56**(9), 930–933.
- Dongmo LS, Villarrubia JS, Jones SN, Renegar TB, Postek MT & Song JF (2000). Experimental test of blind tip reconstruction for scanning probe microscopy. *Ultramicroscopy* 85(3), 141–153.
- Flater EE, Zacharakis-Jutz GE, Dumba BG, White IA & Clifford CA (2014). Towards easy and reliable AFM tip shape determination using blind tip reconstruction. *Ultramicroscopy* 146, 130–143.
- Gołek F, Mazur P, Ryszka Z & Zuber S (2014). AFM image artifacts. Appl Surf Sci 304, 11–19.
- Hübner U, Morgenroth W, Meyer HG, Sulzbach T, Brendel B & Mirandé W (2003). Downwards to metrology in nanoscale: Determination of the AFM tip shape with well-known sharp-edged calibration structures. Appl Phys A 76(6), 913–917.
- Josep C-F, Eugenio C, Alicia F-A & Elena P-C (2014). Correction of the tip convolution effects in the imaging of nanostructures studied through scanning force microscopy. *Nanotechnology* 25(39), 395703.

- Keller D (1991). Reconstruction of STM and AFM images distorted by finitesize tips. Surf Sci 253(1), 353–364.
- Kondratov AV, Rogov OY & Gainutdinov RV (2017). AFM reconstruction of complex-shaped chiral plasmonic nanostructures. *Ultramicroscopy* 181, 81–85.
- Lui CH, Liu L, Mak KF, Flynn GW & Heinz TF (2009). Ultraflat graphene. Nature 462, 339–341.
- Montelius L & Tegenfeldt JO (1993). Direct observation of the tip shape in scanning probe microscopy. *Appl Phys Lett* **62** (21), 2628–2630.
- Reiss G, Schneider F, Vancea J & Hoffmann H (1990). Scanning tunneling microscopy on rough surfaces: Deconvolution of constant current images. *Appl Phys Lett* 57(9), 867–869.
- Ricci D & Braga PC (2004). Recognizing and avoiding artifacts in AFM imaging. In *Atomic Force Microscopy: Biomedical Methods and Applications*, Braga PC & Ricci D (Eds.), pp. 25–37. Totowa, New Jersey: Humana Press.
- Scienceofsharp (2015). The pasted strop Part 3. Available at https://scienceofsharp.wordpress.com/2015/03/31/the-pasted-strop-part-3/ (retrieved May 05, 2019).
- Severin N, Dorn M, Kalachev A & Rabe JP (2011). Replication of single macromolecules with graphene. Nano Lett 11(6), 2436–2439.
- Shen J, Zhang D, Zhang F-H & Gan Y (2017). AFM tip-sample convolution effects for cylinder protrusions. Appl Surf Sci 422, 482–491.
- **Tranchida D, Piccarolo S & Deblieck RAC** (2006). Some experimental issues of AFM tip blind estimation: The effect of noise and resolution. *Meas Sci Technol* **17**(10), 2630–2636.
- Villarrubia JS (1994). Morphological estimation of tip geometry for scanned probe microscopy. *Surf Sci* **321**(3), 287–300.
- Villarrubia JS (1997). Algorithms for scanned probe microscope image simulation, surface reconstruction, and tip estimation. J Res Natl Inst Stand Technol 102(4), 425–454.
- Winzer AT, Kraft C, Bhushan S, Stepanenko V & Tessmer I (2012).

 Correcting for AFM tip induced topography convolutions in protein–DNA samples. *Ultramicroscopy* 121, 8–15.